Journal of Structural Biology 195 (2016) 179–189

Contents lists available at ScienceDirect

Journal of Structural Biology

journal homepage: www.elsevier.com/locate/yjsbi

Intrinsic aggregation propensity of the CsgB nucleator protein is crucial for curli fiber formation

Nikolaos N. Louros, Georgios M.P. Bolas, Paraskevi L. Tsiolaki, Stavros J. Hamodrakas, Vassiliki A. Iconomidou *

Department of Cell Biology and Biophysics, Faculty of Biology, University of Athens, Panepistimiopolis, Athens 157 01, Greece

ARTICLE INFO

Article history:
Received 20 January 2016
Received in revised form 26 May 2016
Accepted 28 May 2016
Available online 28 May 2016

Keywords:
'Aggregation-prone' peptides
Functional amyloid
Homology modeling
Amyloid fibril structure
Biofilms

ABSTRACT

Several organisms exploit the extraordinary physical properties of amyloid fibrils forming natural protective amyloids, in an effort to support complex biological functions. Curli amyloid fibers are a major component of mature biofilms, which are produced by many *Enterobacteriaceae* species and are responsible, among other functions, for the initial adhesion of bacteria to surfaces or cells. The main axis of curli fibers is formed by a major structural subunit, known as CsgA. CsgA self-assembly is promoted by oligomeric nuclei formed by a minor curli subunit, known as the CsgB nucleator protein. Here, by implementing AMYLPRED2, a consensus prediction method for the identification of 'aggregation-prone' regions in protein sequences, developed in our laboratory, we have successfully identified potent amyloidogenic regions of the CsgB subunit. Peptide-analogues corresponding to the predicted 'aggregation-prone' segments of CsgB were chemically synthesized and studied, utilizing several biophysical techniques. Our experimental data indicate that these peptides self-assemble in solution, forming fibrils with characteristic amyloidogenic properties. Using comparative modeling techniques, we have developed three-dimensional models of both CsgA and CsgB subunits. Structural analysis revealed that the identified 'aggregation-prone' segments may promote gradual polymerization of CsgB. Briefly, our results indicate that the intrinsic self-aggregation propensity of the CsgB subunit, most probably has a pivotal role in initiating the formation of curli amyloid fibers by promoting the self-assembly process of the CsgB nucleator protein.

1. Introduction

Amyloids are an after-effect of deposition of ordered protein fibrillar arrangements, known as amyloid fibrils (Chiti and Dobson, 2006). Amyloid fibrils are formed by otherwise soluble proteins or peptides that convert under certain conditions into insoluble fibrous aggregates (Dobson, 1999). Impressively, several proteins with important but otherwise unrelated functions have been associated with amyloid deposition, although they have neither sequence nor structural apparent similarities (Sipe et al., 2014). A large number of widespread diseases, such as AL (Amyloid Light-chain), AA (Amyloid A) or ATTR (Transthyretin-related) amyloidosis, neurodegenerative diseases (Alzheimer's, Parkinson's and Creutzfeldt-Jakob's disease among others), type II diabetes and many more are a consequence of unrestrained deposition of amyloid causing tissue damage and degeneration (Sipe et al., 2014). In contrast, accumulated evidence has shown that occasionally organisms spanning from bacteria to humans exploit the extraordinary intrinsic properties of amyloids in order to support fundamental physiological processes (Iconomidou and Hamodrakas, 2008; Shewmaker et al., 2011). Typical examples of functional amyloid include the extracellular protective coats of several organisms (Iconomidou et al., 2000; Louros et al., 2013, 2014a, 2016b), the intracellular Pmel17 template which is utterly important for the biosynthesis of melanin (Fowler et al., 2006; Louros and Iconomidou, 2015; Louros et al., 2016a) and the formation of biofilms by gram negative bacteria (Hammar et al., 1995).

Bacteria are able to survive and colonize in a diverse variety of environments. Key feature to their resilience is their ability to grow in colonies and produce a complex matrix of extracellular polymeric substances (Donlan, 2002). Using this matrix, bacteria are able to sculpt three-dimensional structures, called biofilms, which shelter the inhabitants from environmental stress (Donlan, 2002). In the case of many *Enterobacteriaceae* such as *Escherichia coli* or *Salmonella enterica*, the major proteinaceous component of this matrix consists of fibers called *curli* that are involved in cell-surface and cell-cell contacts and adhesion (Barnhart and

* Corresponding author.
E-mail address: veconom@biol.uoa.gr (V.A. Iconomidou).

http://dx.doi.org/10.1016/j.jsb.2016.05.012
1047-8477/

Chapman, 2006). Curli fibers exhibit characteristic properties of amyloid fibrils (Chapman et al., 2002) and are composed of two basic proteins; namely, a major structural subunit, known in *E. coli* as CsgA, and a minor subunit serving also as a nucleator protein, known as CsgB, both encoded by a common operon (Hammar et al., 1996, 1995). The two proteins are of identical size (151aa) and comprise similar structural segments (Hammar et al., 1996). Specifically, CsgA and CsgB are built up of three regions, namely a signal peptide, an N-terminal chaperone-binding peptide segment and five consecutive repeat subunits, composed of 22–23 residues, which constitute the amyloid core of curli fibers (Hammer et al., 2007; Wang and Chapman, 2008). Each repeat is composed of a strand-loop-strand motif predicted to form two parallel β-sheets (Wang and Chapman, 2008; Wang et al., 2008).

Both proteins are capable of forming fibers *in vitro*, however detailed evidence indicates that CsgB forms fibers with a significantly faster rate (Hammar et al., 1996). Additionally, the aggregation kinetics of CsgA is accelerated in the presence of CsgB (Hammer et al., 2012). However, *in vivo* curli fibers can only be formed in the presence of both subunits (Barnhart and Chapman, 2006; Blanco et al., 2012; Hammer et al., 2012; Wang et al., 2007), accumulated at ratios approximately 20:1 (CsgA:CsgB) (Van Gerven et al., 2015; White et al., 2001). Furthermore, detailed immunoelectron microscopy studies have shown that CsgB can form short polymers on the cell surface in the absence of CsgA (Bian and Normark, 1997). Finally, CsgB has been proposed to be responsible for creating the initial oligomers/nuclei acting as templates and inducing the polymerization of CsgA, which self-assembles forming the major axis of the curli fiber (Hammer et al., 2007; Shu et al., 2012).

Experimental and theoretical evidence has indicated that amyloid formation is induced by specific short sequence regions of a polypeptide chain that are prone to aggregation, hence regulating the overall aggregation tendency of the protein (Lopez de la Paz and Serrano, 2004; Louros et al., 2015a,b; Teng et al., 2012). In this work, we have identified six individual aggregation-potent regions of the minor curli subunit, by comparing the amyloidogenic profile of both CsgA and CsgB curli proteins of *E. coli*. Structural studies of peptide-analogues corresponding to the identified regions indicate their ability to self-assemble forming fibrils with characteristic amyloidogenic features. Our findings suggest that the 'aggregation-prone' segments could probably be responsible for the ability of CsgB to self-assemble in faster rates than CsgA, *in vitro*, and may also promote the nucleation capabilities of the former. Finally, based on our results, we propose a possible mechanism for both the *in vivo* and *in vitro* curli fiber self-assembly process, by attempting to shed some light on the vague and complicated nucleation process of curli fibers.

2. Materials and methods

2.1. Aggregation propensity sequence analysis of CsgA and CsgB

Protein sequences of CsgA and CsgB from *E. coli* were obtained from Uniprot (Accession Numbers: P28307 and P0ABK7). Initially, the Sec-signal peptide and the 22-residue long N-terminal domain that precedes 5 imperfect repeats in both CsgA and CsgB (Fig. S1) were removed. In order to track down the aggregation propensity of both curli subunits, we implemented AMYLPRED2, a consensus aggregation propensity prediction tool, which was developed by our lab (Tsolis et al., 2013), on the remaining sequence segments of CsgA and CsgB, corresponding to the 5 imperfect repetitive segments that have been associated with the formation of the curli fiber axis. As a consensus tool, AMYLPRED2 takes into account several properties in order to produce a multivariate prediction of sequence amyloidogenicity. Among others, AMYLPRED2 incorporates algorithms which specialize in identifying sequence-specific segments with increased amyloidogenicity (Conchillo-Sole et al., 2007; Maurer-Stroh et al., 2010; Tian et al., 2009), algorithms focused in identifying beta-strand propensity or chameleon "conformational switches" (Hamodrakas, 1988; Kim et al., 2009), and prediction algorithms based on average packing density and hydrophobicity of sequence stretches (Fernandez-Escamilla et al., 2004; Galzitskaya et al., 2006).

2.2. Peptide synthesis and preparation of amyloid fibrils

Six regions of CsgB exhibiting increased aggregation propensity were predicted, namely AAIIGQ$_{46–52}$, LLAVVA$_{67–72}$, NLAYI$_{89–93}$, TAMIIQ$_{112–117}$, AIVVQ$_{135–139}$ and MAIRV$_{144–148}$ (Fig. 1). As a result, peptide-analogues of the predicted segments were synthesized by GeneCust Europe, Luxembourg (purity >98%, free N- and C-terminals). The synthesized CsgB peptide-analogues were dissolved in distilled water (pH 5.75), at a concentration of 10 mg/ml. After incubation for 1–2 weeks, all peptides self-assembled forming either mature amyloid-like fibril-containing gels or lamellar microcrystals composed of such fibrils.

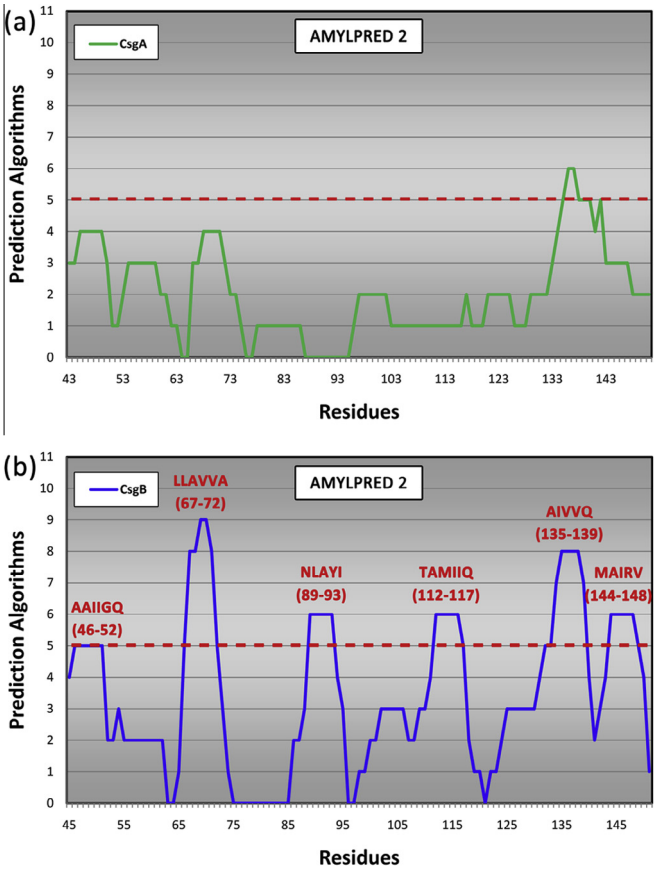

Fig. 1. Amyloidogenic profile of (a) CsgA (green line) and (b) CsgB (blue line). The horizontal axis indicates the number of residues corresponding to the amyloid-forming segments of CsgA and CsgB, containing five individual repetitive segments each, whereas the vertical axis corresponds to the number of individual prediction algorithms utilized by AMYLPRED2. AMYLPRED2 has a default cut-off value of successful aggregation propensity prediction by at least 5 out of 11 algorithms (shown by red line). CsgB has an apparent increased aggregation propensity, in comparison to CsgA where only minimal propensity in observed. Six individual, more or less hydrophobic, segments of CsgB are identified, namely AAIIGQ$_{46–52}$, LLAVVA$_{67–72}$, NLAYI$_{89–93}$, TAMIIQ$_{112–117}$, AIVVQ$_{135–139}$ and MAIRV$_{144–148}$. The equivalent distance between the first 5 predicted segments (21–23 residues) implies that the individual repeats of CsgB have a common amyloidogenic profile.

2.3. Transmission electron microscopy (TEM) and negative staining

A drop (~5 μl) of each fibril-containing solution was applied to glow-discharged 400-mesh carbon-coated copper grids, for 60 s. The grids were flash-washed with distilled water and stained with a drop of 2% (w/v) aqueous uranyl acetate for 60 s. Excess stain was removed by blotting with a filter paper. The fibril containing grids were initially air dried and examined with a Morgagni™ 268 transmission electron microscope, operated at 80 kV. Digital acquisitions were performed with an 11 Megapixel side-mounted Morada CCD camera (Soft Imaging System, Muenster, Germany).

2.4. X-ray diffraction

A droplet (10 μl) of each peptide solution, containing self-assembled amyloid-like fibrils, was placed between two aligned siliconized glass rods, spaced 2 mm apart. The droplets were allowed to dry slowly at ambient conditions, for approximately 1 h, to form oriented fibers suitable for X-ray diffraction. X-ray diffraction patterns for AAIIGQ$_{46–52}$, LLAVVA$_{67–72}$ and TAMIIQ$_{112–117}$ peptides were collected, using a SuperNova-Agilent Technologies X-ray generator equipped with a 135-mm ATLAS CCD detector and a 4-circle kappa goniometer, at the Institute of Biology, Medicinal Chemistry and Biotechnology, National Hellenic Research Foundation (CuK_α high intensity X-ray micro-focus source, λ = 1.5418 Å), operated at 50 kV, 0.8 mA. The specimen-to-film distance was set at 52 mm. The exposure time was set to 400 s. The X-ray diffraction patterns were initially viewed using the program CrysAlisPro (Oxford Diffraction, 2009) and subsequently displayed and measured with the aid of the program iMosFLM (Leslie and Powell, 2007). The X-ray diffraction patterns for NLAYI$_{89–93}$, AIVVQ$_{135–139}$ and MAIRV$_{144–148}$ were collected at the P14 beamline, at a wavelength of 1.23953 Å (Petra III, EMBL-Hamburg, Germany) using a PILATUS 6M detector. The detector distance was set to 225.11 mm and exposure times were set to 1 s. The X-ray diffraction patterns were displayed and measured using iMosFLM.

2.5. Congo red staining and polarized light microscopy

Fibril suspensions of each peptide-analogue solution were applied to glass slides and were air-dried at ambient conditions. The films produced, containing amyloid-like fibrils, were stained with a 1% Congo red solution in distilled water (pH 5.75) for 20 min (Louros et al., 2015a, 2014b; Romhanyi, 1971). Excess stain was removed through tap water washes (Romhanyi, 1971). The samples were observed under bright field illumination and between crossed polars, using a Leica MZ75 polarizing stereomicroscope equipped with a JVC GC-X3E camera.

2.6. Attenuated total reflectance Fourier-transform infrared spectroscopy (ATR FT-IR) and post-run spectra computations

Drops (~10 μl) of the CsgB peptide-analogue solutions were cast on flat stainless steel plates coated with an ultrathin hydrophobic layer (SpectRIM, Tienta Sciences, Inc., Indianapolis, USA) and left to dry slowly at ambient conditions to form a thin film. IR spectra were obtained at a resolution of 4 cm^{-1}, utilizing an IR microscope (IRScope II, BrukerOPTICS, BrukerOptik GmbH, Ettlingen, Germany), equipped with a Ge ATR objective lens (20×) and attached to a FT-IR spectrometer (Equinox 55, BrukerOPTICS). Ten 32-scan spectra were collected from each sample and averaged to improve the S/N ratio. All spectra are shown in the absorption mode, after correction for the wavelength-dependence of the penetration depth (d_p analogous λ). Derivatives were computed analytically using routines of the Bruker OPUS/OS2 software including smoothing over a ±13 cm^{-1} range around each data point, performed by the Savitsky-Golay algorithm (Savitsky and Golay, 1964). Smoothing over narrower ranges resulted in deterioration of the S/N ratio and did not increase the number of minima that could be determined with confidence. The minima in the second derivative were used to determine the corresponding absorption band maxima (data not shown).

2.7. Comparative modeling

Sequences of CsgA, CsgB (*E. coli*), AgfA and AgfB (*Salmonella enteritidis*) proteins (Accession Numbers: P28307, P0ABK7, P0A1E7 and P0A1E9, respectively) were extracted from Uniprot. Sequence alignment was performed using ClustalW (Thompson et al., 1994) (Fig. S2). Models of the three-dimensional structures of CsgA (Fig. S3) and CsgB (Fig. S4) were derived by performing sequence threading, utilizing MODELLER 9v2 (Eswar et al., 2006), using the previously proposed structural models of AgfA and AgfB (Collinson et al., 1999; White et al., 2001) as templates. Finally, the derived models were minimized utilizing the MMTK toolkit (Hinsen, 2000), included in the Chimera molecular graphics system (Pettersen et al., 2004) and subsequently evaluated with DSSP and the WHATIF package (Vriend, 1990).

2.8. Docking and nucleation modeling

The model of the CsgB protein was used to perform docking experiments, in order to evaluate the position of the predicted 'aggregation-prone' peptides as a potential interface for curli polymerization. The HADDOCK version 2.1 was used with unambiguously defined interaction restraints to drive the docking (de Vries et al., 2010). Initially, a CsgB dimer was constructed by specifying residues of the first and last repeat as active residues. Secondly, docking with defined interaction restraints based on our experimental results was also performed. Specifically, the self-aggregating AAIIGQ$_{46–52}$, LLAVVA$_{67–72}$, NLAYI$_{89–93}$, TAMIIQ$_{112–117}$, AIVVQ$_{135–139}$ motifs were defined as active residues. Finally, a set of docking experiments with defined interaction restraints was also performed for CsgA, specifying residues of the homologous to the identified CsgB 'aggregation-prone' regions as active residues. Monomer register was undefined during all docking procedures. Structure calculations were performed by CNS1.2 (Brunger et al., 1998), whereas non-bonded interactions were calculated with the OPLS force field (Jorgensen and Tirado-Rives, 1988) using an 8.5 Å cutoff. The solvated docking protocol was favored, since in comparison to unsolvated docking it may yield higher quality docking predictions (Kastritis et al., 2011).

3. Results and discussion

3.1. CsgB exhibits increased aggregation propensity compared to CsgA

The aggregation potency of both the major and minor subunit of *E. coli* curli fibers was calculated and analyzed utilizing AMYLPRED2. Impressively, although the aforementioned sequences share relatively high sequence homology, significant differences emerge regarding their aggregation tendency. As the results of AMYLPRED2 clearly indicate, severely lower aggregation potency was predicted for CsgA in comparison to CsgB, since the former only presents segments with an extraneous minor aggregation propensity (Fig. 1a). In contrast, CsgB presents six individual segments, with high self-aggregating potential, coinciding more or less with the aforementioned segments of the CsgA subunit (Fig. 1b). The CsgB segments are composed primarily of hydrophobic residues, the burial of which may promote the aggregation potency of CsgB. Remarkably, the homologous regions located in

CsgA have several polar or charged residues that may hinder a similar aggregation effect for the CsgA subunit. Finally, with the exception of the last predicted 'aggregation-prone' section ($MAIRV_{144–148}$), the predicted segments exhibit an evident repetition, emerging every 21–23 residues. By taking into account the fact that CsgB repeats comprise 22–23 residues, this observation indicates that the five repetitive units of CsgB have a similar amyloidogenic profile, therefore, could contribute equally to the aggregation potency of the minor curli subunit. In summary, it appears that the increased intrinsic aggregation propensity of CsgB, compared to CsgA, corroborates its necessity for the nucleation process during curli fiber biogenesis.

3.2. A β-helical model reveals the formation of a potential CsgB 'aggregation-prone' interface

Previous elegant studies have reported a three-dimensional model of AgfA and AgfB curli subunits of *S. enteritidis* (Collinson

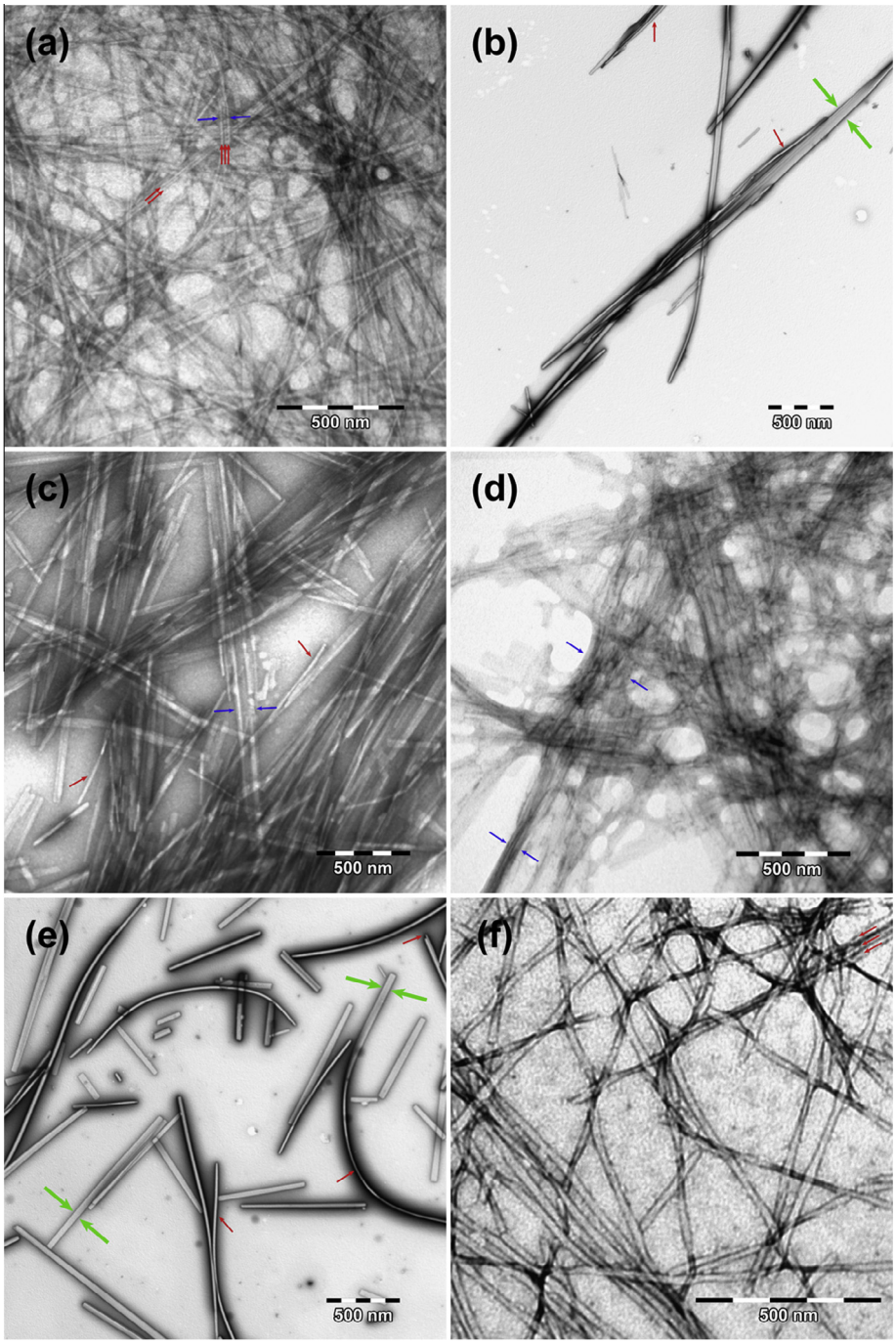

Fig. 2. Electron micrographs of amyloid-like fibrils formed after self-assembly of the (a) $AAIIGQ_{46–52}$, (b) $LLAVVA_{67–72}$, (c) $NLAYI_{89–93}$, (d) $TAMIIQ_{112–117}$, (e) $AIVVQ_{135–139}$ and (f) $MAIRV_{144–148}$ 'aggregation-prone' peptides. Amyloid-like fibrils composed of the (a) $AAIIGQ_{46–52}$, (c) $NLAYI_{89–93}$, (d) $TAMIIQ_{112–117}$ and (f) $MAIRV_{144–148}$ peptides appear straight and unbranched, with indeterminate lengths and a tendency to coalesce laterally forming fibril batches or ribbons with variable thickness (blue arrows). The widths of the $AAIIGQ_{46–52}$ and $NLAYI_{89–93}$ derived fibrils are approximately 100–120 Å, whereas for the $TAMIIQ_{112–117}$ and $MAIRV_{144–148}$ peptides they are approximately 150–200 Å, respectively (highlighted in red arrows). In the case of (b) $LLAVVA_{67–72}$ and (e) $AIVVQ_{135–139}$, peptides, long and unconnected fibrils with diameters of 100–150 Å are formed (shown in red arrows). However, in both cases, the fibrils appear to have increased lateral attachments forming lamellar one-dimensional crystal-like structures of various diameters (shown in green arrows). Scale bars were set to 500 nm.

et al., 1999; White et al., 2001). These structural predictions were further supported by recent complementary evidence derived through sequence variation analysis (Tian et al., 2015). Based on the above and the fact that AgfA and AgfB share high sequence homology to CsgA and CsgB (Fig. S2), respectively (more than 70% sequence identity), a three-dimensional model of both the major and minor curli subunit of *E. coli* was derived, by performing sequence threading, utilizing the proposed AgfA and AgfB models as template structures. Analysis of the derived models indicates that both curli subunits fold into a right-handed β-helical structure composed of five individual structural segments (R1–R5) (Figs. S3 and S4). Each individual segment, corresponding to one of the five repetitive segments of CsgA and CsgB, has a β-hairpin-like structure (β-strand-loop-β-strand motif) and winds around the β-helix axis forming two parallel facing β-sheets (Figs. S3 and S4). Both β-helical structures exhibit typical characteristics of the β-solenoid fold, since they have a compact hydrophobic core and are stabilized by the formation of individual hydrogen bond ladders (H-ladders), shaped by stacked conserved polar residues along the β-helical axis (Figs. S3 and S4). Specifically, two Gln and one Asn and Ser H-bond ladders are formulated in both CsgA and CsgB, with the Gln and Asn ladders formed at common conserved positions of both subunits (Figs. S3 and S4). Based on the above, both curli subunits apparently share several common structural characteristics. However, impressive differences emerge regarding their potential aggregation propensity. The predicted 'aggregation-pro ne' peptides of CsgB coincide with major parts of β-strands of each individual repeat. More specifically, five out of the six predicted

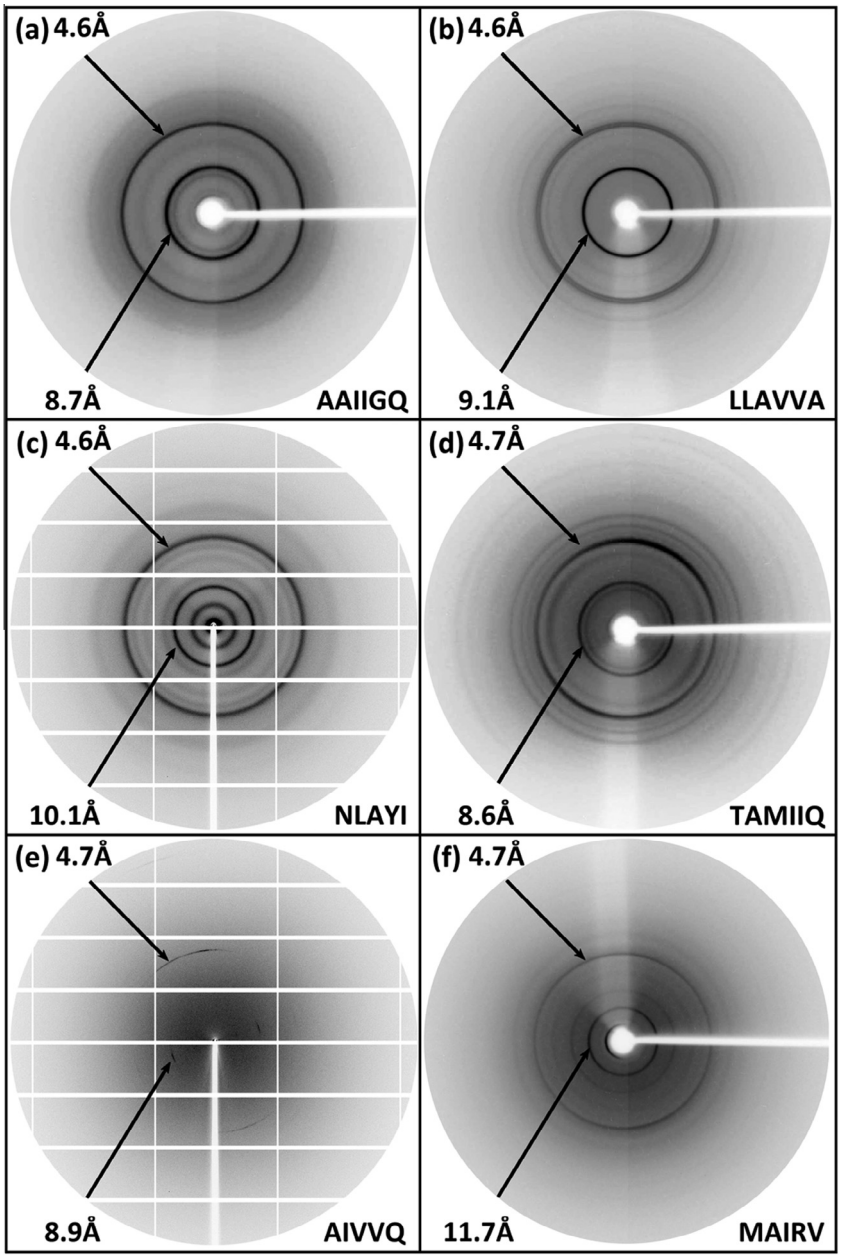

Fig. 3. X-ray diffraction patterns of oriented fibers, containing more or less aligned amyloid fibrils, derived by the self-assembled peptides. The patterns exhibit the typical to a 'cross-β'-like architecture reflections. Specifically, the 4.6–4.7 Å structural repeat arises from the distance between β-strands aligned perpendicularly to the fiber axis, whereas the 8.7, 9.1, 10.1, 8.6, 8.9 and 11.7 Å periodicities correspond to the packing distance of β-sheets running parallel to the fiber axis for the (a) $AAIIGQ_{46-52}$, (b) $LLAVVA_{67-72}$, (c) $NLAYI_{89-93}$, (d) $TAMIIQ_{112-117}$, (e) $AIVVQ_{135-139}$ and (f) $MAIRV_{144-148}$ 'aggregation-prone' peptides, respectively. Reflections may appear as rings due to poor alignment of the oriented fiber constituent fibrils.

segments, namely, AAIIGQ$_{46–52,}$ LLAVVA$_{67–72}$, NLAYI$_{89–93}$, TAM IIQ$_{112–117}$ and AIVVQ$_{135–139}$ segments shape a potential hydrophobic interface, extended along the β-helical axis and running along the one β-sheet side of the CsgB β-solenoid structure (Figs. S4a and S5b). In CsgA, this hydrophobic interface is disrupted by the presence of polar and charged residues of the homologous segments (Fig. S5a, c and e). Certain of the aforementioned residues have been previously highlighted as possible gatekeeper residues modulating the aggregation tendency of CsgA (Wang et al., 2010). The increased hydrophobicity and aggregation potential of the CsgB interface may be the driving force behind nucleation of the minor curli subunit, thus rendering it utterly important for *in vivo* formation of curli fibers.

3.3. Formation of amyloid-like fibrils by CsgB 'aggregation-prone' segments

Based on our modeling results, we sought to experimentally investigate whether the predicted 'aggregation-prone' segments indeed possess the ability to self-aggregate into fibrils with amyloidogenic properties. For this reason, all predicted peptides were examined after synthesis and were found to form fibril-containing gels. Specifically, after incubation for 1–2 weeks in distilled water (pH 5.75), all peptide-analogues of CsgB self-aggregate forming fibrillar arrangements that appear straight and unconnected, with indeterminate lengths, and widths that range from 100 to 200 Å between different peptides, respectively (Fig. 2, red arrows). Amyloid-like fibrils formed by the AAIIGQ$_{46–52}$ peptide occasionally interact in a lateral fashion leading to the formation of striated ribbons composed of two to several fibrils, whereas in the case of NLAYI$_{89–93}$, TAMIIQ$_{112–117}$ and MAIRV$_{144–148}$ peptides, individual fibrils interact laterally forming ribbons or batches of fibrils with variable thickness (Fig. 2, blue arrows). In respect to the LLAVVA$_{67–72}$ and AIVVQ$_{135–139}$ peptides, the derived amyloid-like fibrils have strong lateral attachments and as a result lead towards the formation of lamellar one-dimensional crystal-like structures (Fig. 2, green arrows), although no layer lines were reported through the X-ray diffraction analysis (Fig. 3). These observations are in line with studies suggesting that common mechanisms underlie behind amyloid fibrillation and protein crystallization events and with similar structures, which have been reported for several other amyloid fibril-forming segments in the past (Ivanova et al., 2009; Kitayama et al., 2013; Wiltzius et al., 2008).

3.4. Amyloid-like fibrils possess characteristics of a "cross-β" structure

Aligned fibers, composed of oriented fibrils, derived from the self-assembling peptide solutions, produce X-ray diffraction patterns containing reflections of the typical "cross-β" architecture of amyloid fibrils (Fig. 3) (Geddes et al., 1968; Sunde et al., 1997). More specifically, X-ray diffraction patterns derived from all 'aggregation-prone' peptides present a relatively strong meridional reflection, indicative of a 4.6–4.7 Å structural periodicity, which is assigned to the inter-chain distance between successive hydrogen bonded β-strands, ordered perpendicularly to the fibril axis. Moreover, a second strong equatorial reflection, appearing at 8.7, 9.1, 10.1, 8.6, 8.9 and 11.7 Å for the AAIIGQ$_{46–52,}$ LLAVVA$_{67–72}$, NLAYI$_{89–93}$, TAMIIQ$_{112–117}$, AIVVQ$_{135–139}$ and MAIRV$_{144–148}$ peptides, respectively, is ascribed to the variable packing distance between packed β-sheets, aligned parallel to the fiber axis. Reflections of the AAIIGQ$_{46–52,}$ LLAVVA$_{67–72}$, and NLAYI$_{89–93}$ patterns appear as rings due to poor alignment of the oriented fiber constituent fibrils.

Complementary evidence was derived by spectral acquisition, utilizing ATR FT-IR spectroscopy, an experimental technique used for the analysis of the secondary structure of proteins or peptides associated with the formation of amyloid fibrils, without the drawbacks associated with more conventional vibrational techniques (Iconomidou et al., 2001; Kong and Yu, 2007). The ATR FT-IR spectra reveal a prominent amide I band, located at 1632, 1630, 1636, 1632, 1630 and 1629 cm^{-1} for the AAIIGQ$_{46–52,}$ LLAVVA$_{67–72}$, NLAYI$_{89–93}$, TAMIIQ$_{112–117}$, AIVVQ$_{135–139}$ and MAIRV$_{144–148}$ peptides, respectively, suggesting a β-sheet secondary structure (Table 1). The sharpness of the observed amide I bands is indicative of uniformity in the β-sheet structure, suggesting that the range of the phi and psi angles in the β-sheets is relatively limited (Fig. 4). The amide II components shown for the AAIIGQ$_{46–52,}$ NLAYI$_{89–93}$, TAMIIQ$_{112–117}$, AIVVQ$_{135–139}$ and MAIRV$_{144–148}$ peptides (Table 1), also imply the presence of a β-sheet secondary structure (Cooper and Knutson, 1995; Krimm and Bandekar, 1986). Finally, the additional shoulders at 1690–1693 cm^{-1}, observed in each spectrum suggest that the β-sheets are arranged in an antiparallel fashion (Surewicz et al., 1993).

Table 1
Bands observed in the ATR FT-IR spectra produced from hydrated films of all the CsgB 'aggregation-prone' peptides, after self-assembly and formation of amyloid-like fibrils, and their tentative assignments (Fig. 4).

Bands (cm^{-1})						Assignment
AAIIGQ	LLAVVA	NLAYI	TAMIIQ	AIVVQ	MAIRV	
1136	1138	1136	1136		1132	TFA
1180		1190			1180	TFA
1201	1209	1207	1204		1203	TFA
		1230				β-Sheet (Amide III)
		1516				Tyr
1531		1553	1541	1552	1537	β-Sheet (Amide II)
1632	1630	1636	1632	1630	1629	β-Sheet (Amide I)
1663	1678	1665	1663	1670	1670	TFA
1692	1692	1693	1692	1690	1693	Antiparallel β-sheet

Deposits of fibrils from all the peptide–analogues were stained with the diagnostic Congo red dye, which is widely used in order to detect the presence of amyloid (Divry and Florkin, 1927; Missmahl and Hartwig, 1953). Evidently, as observed under bright field illumination of a polarizing microscope, all peptide deposits bind the amyloid-specific Congo red dye, therefore indicating the amyloidogenic properties of fibrils formed by the self-assembling peptides (Fig. 5). Furthermore, the amyloid properties of the fibrils are certified, under crossed polars of the polarizing microscope, where the characteristic apple/green birefringence, consistently shown from Congo red stained amyloid deposits, is exhibited (Fig. 5).

All identified 'aggregation-prone' segments of CsgB have an inherent ability to self-assemble forming structures with distinct amyloidogenic properties and a "cross-β" structure. Following detailed studies suggesting that motifs composed of 6–8 residues, derived from β-continuous interfaces of oligomeric proteins, have an intrinsic self-aggregation propensity by retaining the polymerizing properties of their parental protein interfaces (Valery et al., 2013), our experimental results suggest that the parental hydrophobic CsgB interface could retain the characteristic amyloidogenic properties of its individual filial components, namely the AAIIGQ$_{46–52,}$ LLAVVA$_{67–72}$, NLAYI$_{89–93}$, TAMIIQ$_{112–117}$ and AIVVQ$_{135–139}$ segments.

3.5. 'Aggregation-prone' segments possibly promote nucleation of CsgB

The β-solenoid fold has been extensively highlighted as a potent polymerization component of amyloid-forming proteins (Downing and Lazo, 1999; Lazo and Downing, 1998, 1999). This process has been proposed to take part through head-to-tail interactions formed between exposed terminal coils presenting increased

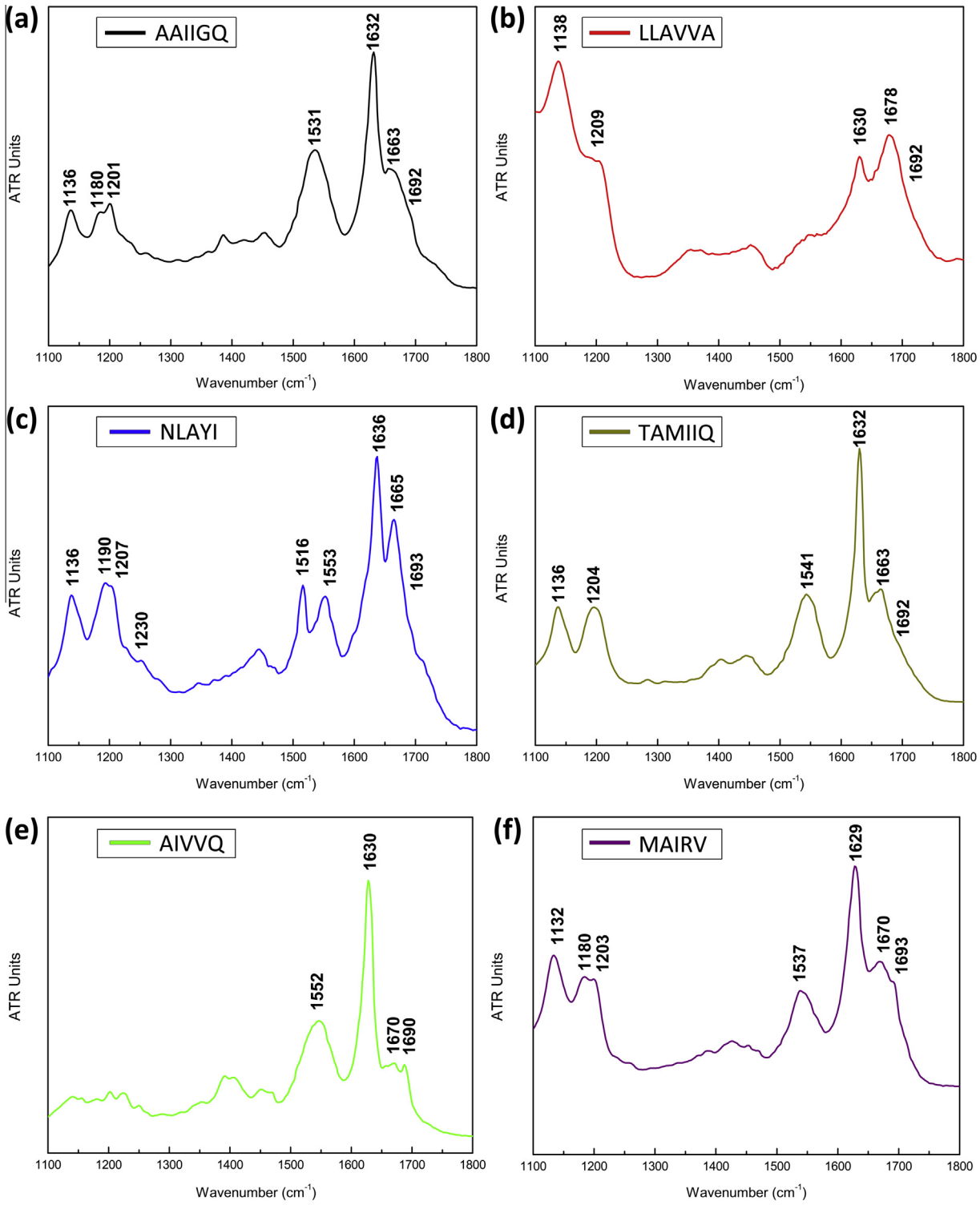

Fig. 4. ATR FT-IR (1100–1800 cm^{-1}) spectra. The derived spectra were obtained from thin hydrated-films containing amyloid-like fibrils, contained within solutions of the (a) $AAIIGQ_{46-52}$, (b) $LLAVVA_{67-72}$, (c) $NLAYI_{89-93}$, (d) $TAMIIQ_{112-117}$, (e) $AIVVQ_{135-139}$ and (f) $MAIRV_{144-148}$ peptides, respectively. All resulting spectra are indicative of the preponderance of an antiparallel β-sheet secondary structure (Table 1).

H-bonding complementarity, leading to the formation of fibrils with indefinite length, such as amyloid fibrils (Kajava and Steven, 2006; Richardson and Richardson, 2002). This notion is also supported by accumulating evidence proposing that this process is frequently interrupted by the presence of capping motifs at the terminal repeat segments, composed of proline residues, β-bulges and other bulky moieties preventing integrative H-bonding between monomers (Bryan et al., 2011; Richardson and Richardson, 2002). The amino acid composition of the CsgB N- and C-terminal repetitive segments does not introduce any of the above characteristics. Consequently, a CsgB dimer was constructed, clearly demonstrating that dimerization of the β-helical monomers occurs by hydrogen bond complementarity between the edge β-strands of the R1 and R5 repeats of each monomer (Fig. 6). Both

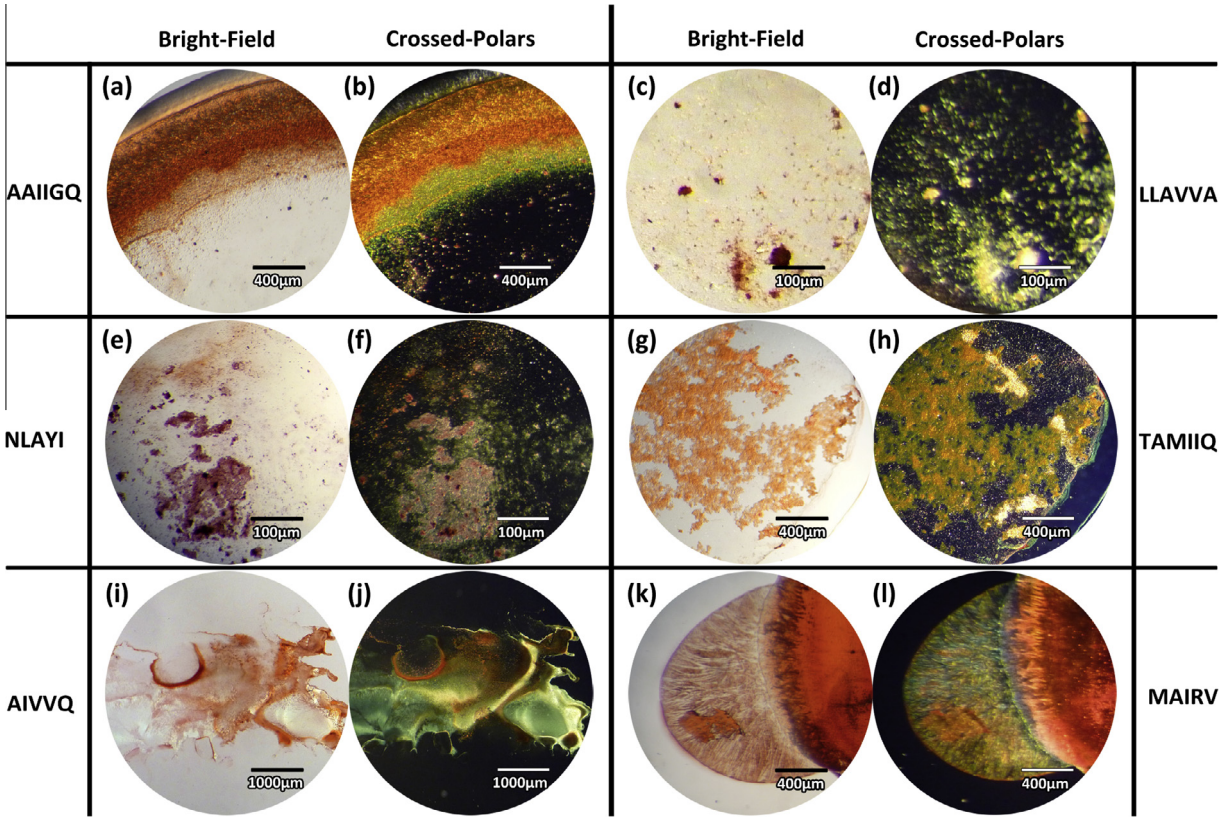

Fig. 5. Congo-red staining of (a, b) $AAIIGQ_{46–52}$, (c, d) $LLAVVA_{67–72}$, (e, f) $NLAYI_{89–93}$, (g, h) $TAMIIQ_{112–117}$, (i, j) $AIVVQ_{135–139}$ and (k, l) $MAIRV_{144–148}$, peptide-derived amyloid deposits. (a, c, e, g, i, k) Fibril-containing gels from all peptides bind the amyloid-specific Congo red dye, as seen under bright-field illumination and (b, d, f, h, j, l) exhibit the characteristic for amyloid apple/green birefringence under crossed-polars of a polarizing microscope.

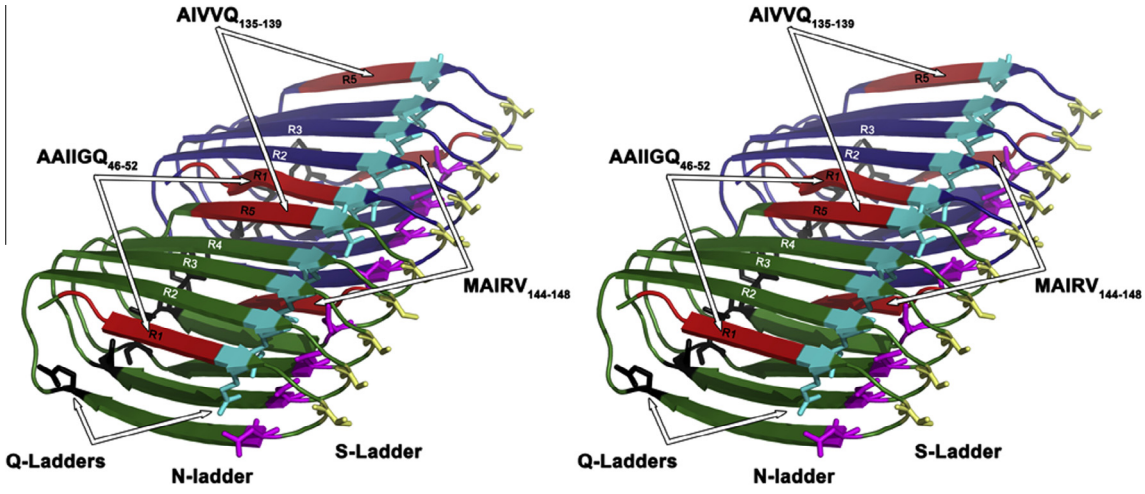

Fig. 6. Stereo view representation of CsgB dimers, derived by driven docking experiments, using HADDOCK, with residues of the first and last CsgB repeat, namely R1 and R5, as active residues. A β-solenoid structure is formed through head-to-tail interactions, forming complementary hydrogen bonds between the β-strands of the R1–R5 edge repetitive segments of individual monomers (shown in blue and green, respectively). It is intriguing that, three out of six identified 'aggregation-prone' segments, namely $AAIIGQ_{48–52}$, $AIVVQ_{135–139}$ and $MAIRV_{144–148}$ (shown in red), are major parts of the edge segments participating in the dimerization. The β-solenoid axis is further stabilized by the extension of the four individual hydrogen bond ladders observed for the monomers, namely the N-ladder, S-ladder and Q-ladders, shown in sticks and colored in magenta (N-ladder), yellow (S-ladder), cyan (Q-ladder) and black (Q-ladder), respectively.

sections are composed mainly by 'aggregation-prone' segments, specifically the $AAIIGQ_{46–52}$, $AIVVQ_{135–139}$ and $MAIRV_{144–148}$ peptides which are major parts of the edge β-strands and possibly have an important role in the extension of the fibrillar axis. Moreover, the dimer is further stabilized by the extension of the four H-bond ladders of the individual monomers, suggesting that an elongated fibrillar structure with "cross-β" architecture could be formed along the axis of the β-solenoid through head-to-tail interactions between successively stacked monomers.

As already mentioned, five 'aggregation-prone' segments shape a potential hydrophobic interface running along one side of the CsgB β-solenoid structure. Residues corresponding to this specific

interface were set as active residues, during a second round of driven docking experiments. The derived docking results disclosed the formation of dimers sufficiently burying their 'aggregation-prone' interactive surfaces (Fig. S6b). More specifically, a tight hydrophobic core is formed, composed primarily of residues belonging to the identified 'aggregation-prone' region of CsgB, with favorable π-stacking interactions occurring within the center of the core, through stacking of the Y92 side chains of individual monomers. Furthermore, residues K66 and E74 form an intermolecular salt bridge, whereas D94 and K118 form an intramolecular salt bridge, located on each side of the dimer interface, isolating in that manner the tight hydrophobic core (Fig. S6b). In comparison, CsgA dimers are also formed by similar, yet less favorable interactions (Fig. S6a). More specifically, docking results indicated that the extensive polar and charged residues of the CsgA interface could possibly take part in dimerization by forming a network of salt bonds composed by residues D67, H73, D87, D91, R95, E112 and K116 of CsgA. In detail, intermolecular salt bonds could possibly be formed between facing residues D67-H73, D87-R95 and E112-K116, in addition to a possible intramolecular D91-K116 salt bridge (Fig. S6a). Future site-directed mutagenesis studies are required in order to experimentally verify the presence of the aforementioned salt bonds. Although it is possible for both CsgA and CsgB to form dimers with a common interface, docking experiments indicate that more favorable hydrophobic interactions occur during CsgB dimer formation comparing to CsgA.

3.6. A possible in vivo and in vitro polymerization mechanism of curli proteins

A final model was formulated in detail, by combining both CsgB docking derived dimers. For clarity, this structural model was prolonged into a 16-meric model composed of two perpetual β-helical structures that interact via their 'aggregation-prone' interfaces (Fig. 7). The individual β-helical structures, comprising successively stacked CsgB subunits, wind around the main axis and are both stabilized by the extension of the four H-bond ladders reported for the individual monomers. This superstructure can be unlimitedly elongated along the axis of the β-solenoid, leading to the formation of fibrils with indeterminate length, a diameter of approximately 40–60 Å and "cross-β" architecture (Fig. 7). The pitch of the β-helical arrangement is approximately 70 nm long

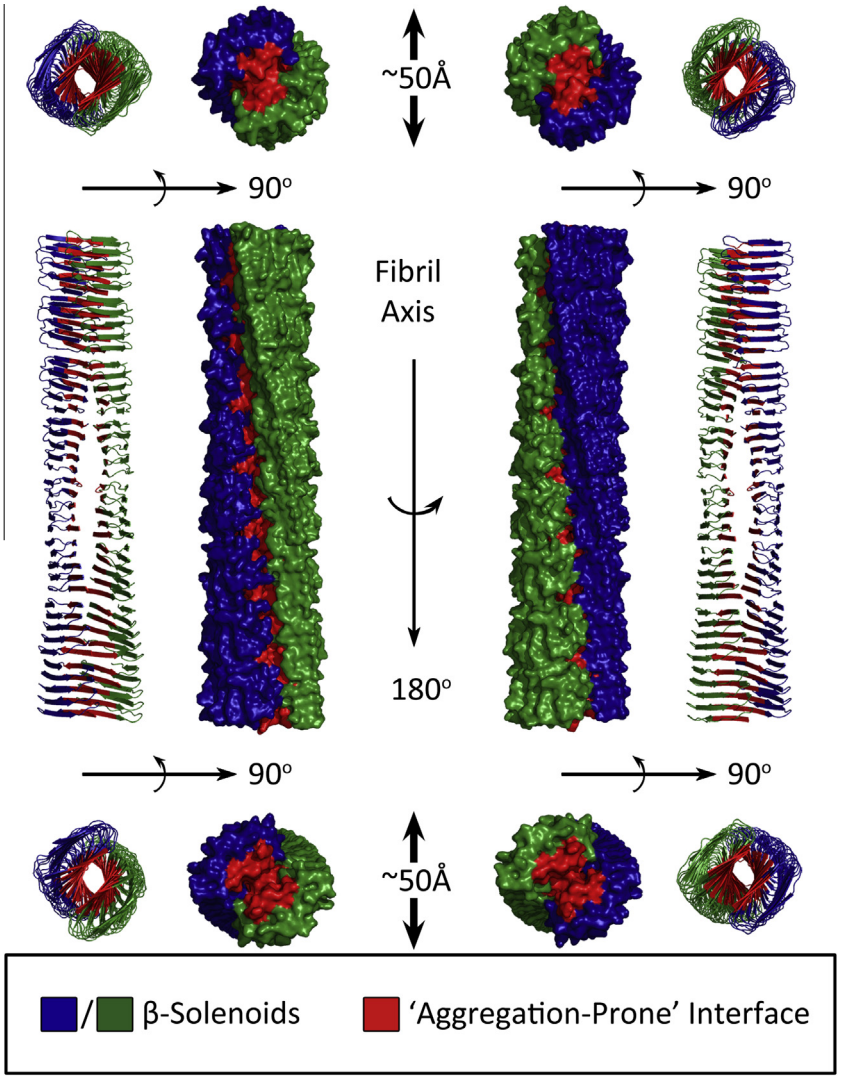

Fig. 7. A model of CsgB self-assembly. Successive CsgB monomers are stacked together with head-to-tail interactions prolonging a perpetual β-solenoid axis (shown in green and blue, as stated by the legend). The β-solenoids are brought together via their aggregation-potent interfaces, composed of the $AAIIGQ_{46-52}$, $LLAVVA_{67-72}$, $NLAYI_{89-93}$, $TAMIIQ_{112-117}$ and $AIVVQ_{135-139}$ 'aggregation-prone' peptides, formulating a superhelical structure with a diameter of approximately 50 Å and a "cross-β" structure, all experimentally verified structural properties of curli amyloid fibers.

and corresponds to 28 successively stacked monomers. Similar properties are ascribed to curli fibers formed by the *Escherichia* and *Salmonella* species, with early and late studies indicating that curli fibers have an indefinite length and widths of approximately 4–6 nm (Cao et al., 2014; Howorka, 2011; Larsen et al., 2007; Shu et al., 2012). The derived model could possibly represent the structure of CsgB amyloid fibers formed *in vitro*, or it could suggest a possible mechanism for the formation of the initial CsgB oligomers, which are important during early nucleation stages of curli fiber biogenesis, by inducing polymerization of CsgA.

Experimental data have elucidated that CsgA and CsgB self-assemble *in vitro*, with the latter aggregating in a shorter lag period (Hammar et al., 1996). Based on the evident structural similarity between CsgA and CsgB (Evans and Chapman, 2013), both proteins may polymerize following a similar self-assembly mechanism (Figs. S7a and b), or by prolonging the initial nuclei formed due to the intrinsic aggregation propensity of CsgB (Figs. S7c). This notion is further supported by concomitant evidence revealing that *in vitro* CsgA polymerization is accelerated in the presence of CsgB (Hammer et al., 2012). Regarding *in vivo* curli fiber formation, studies have shown that the curli fiber axis is composed of both CsgA and CsgB (~20:1), with the former actively secreted to the extracellular matrix, whereas CsgB is mostly located close or bound to the cell surface (Loferer et al., 1997). CsgB localization to the outer membrane remains unknown, however studies reveal that at least one additional component facilitates this process, namely CsgF (Nenninger et al., 2009). Moreover, previous studies have suggested that the C-terminal repeat unit of CsgB has an important role in templating the nucleation process of curli fibers by interacting with the outer bacterial membrane, rendering CsgB important for the nucleation of CsgA (Hammer et al., 2012). Based on the above it could be suggested that, *in vivo*, CsgB initially forms nuclei due to its increased aggregation potency, close to or bound to the cell surface, which serve as templates promoting CsgA self-assembly (Fig. S7d). In any case, the identified high self-aggregation propensity of CsgB might possibly participate in curli fiber biogenesis by regulating the crucial initial nucleation phase of the minor curli subunit both *in vivo* and *in vitro*.

To summarize, the results presented provide insight into the complicated curli fiber formation process by proposing a possible CsgB nucleation mechanism. Information that could shed light into curli amyloid fibril formation are important, since curli fibers are the major template behind the formation of biofilms (DePas and Chapman, 2012) which are associated to antibiotic-resistant microbial strains and have an immense impact in the medical field (Bryers, 2008), in addition to countless biotechnological applications, such as remediation of water pollutants (Singh et al., 2006), pharmaceutical products (Edwards and Kjellerup, 2013), even microbial fuel cells (Zhang et al., 2011).

Funding

The research leading to these results has received partial funding from the European Community's Seventh Framework Programme (FP7/2007-2013) under BioStruct-X (grant agreement N °283570). The infrastructure that the authors used for the present work is associated with the Greek National Research Infrastructure in Structural Biology, Instruct-EL.

Acknowledgements

We thank the Institute of Biology, Medicinal Chemistry and Biotechnology at National Hellenic Research Foundation for hospitality. We acknowledge the help of Dr. Evangelia Chrysina with the X-ray diffraction experiments. The help of Dr. George Baltatzis and Prof. Efstratios Patsouris and the use of the Morgagni Microscope at the 1st Department of Pathology, Medical School, University of Athens are also gratefully acknowledged. We also thank the University of Athens for support. Finally, the authors sincerely thank the Editor-in-Chief for handling this manuscript and the anonymous reviewers for their very valuable and constructive criticism, which helped us to considerably improve the manuscript.

Appendix A. Supplementary data

Supplementary data associated with this article can be found, in the online version, at http://dx.doi.org/10.1016/j.jsb.2016.05.012.

References

Barnhart, M.M., Chapman, M.R., 2006. Curli biogenesis and function. Annu. Rev. Microbiol. 60, 131–147.
Bian, Z., Normark, S., 1997. Nucleator function of CsgB for the assembly of adhesive surface organelles in *Escherichia coli*. EMBO J. 16, 5827–5836.
Blanco, L.P., Evans, M.L., Smith, D.R., Badtke, M.P., Chapman, M.R., 2012. Diversity, biogenesis and function of microbial amyloids. Trends Microbiol. 20, 66–73.
Brunger, A.T., Adams, P.D., Clore, G.M., DeLano, W.L., Gros, P., Grosse-Kunstleve, R. W., Jiang, J.S., Kuszewski, J., Nilges, M., Pannu, N.S., Read, R.J., Rice, L.M., Simonson, T., Warren, G.L., 1998. Crystallography & NMR system: a new software suite for macromolecular structure determination. Acta Crystallogr. D Biol. Crystallogr. 54, 905–921.
Bryan Jr., A.W., Starner-Kreinbrink, J.L., Hosur, R., Clark, P.L., Berger, B., 2011. Structure-based prediction reveals capping motifs that inhibit beta-helix aggregation. Proc. Natl. Acad. Sci. U.S.A. 108, 11099–11104.
Bryers, J.D., 2008. Medical biofilms. Biotechnol. Bioeng. 100, 1–18.
Cao, B., Zhao, Y., Kou, Y., Ni, D., Zhang, X.C., Huang, Y., 2014. Structure of the nonameric bacterial amyloid secretion channel. Proc. Natl. Acad. Sci. U.S.A. 111, E5439–E5444.
Chapman, M.R., Robinson, L.S., Pinkner, J.S., Roth, R., Heuser, J., Hammar, M., Normark, S., Hultgren, S.J., 2002. Role of *Escherichia coli* curli operons in directing amyloid fiber formation. Science 295, 851–855.
Chiti, F., Dobson, C.M., 2006. Protein misfolding, functional amyloid, and human disease. Annu. Rev. Biochem. 75, 333–366.
Collinson, S.K., Parker, J.M., Hodges, R.S., Kay, W.W., 1999. Structural predictions of AgfA, the insoluble fimbrial subunit of *Salmonella* thin aggregative fimbriae. J. Mol. Biol. 290, 741–756.
Conchillo-Sole, O., de Groot, N.S., Aviles, F.X., Vendrell, J., Daura, X., Ventura, S., 2007. AGGRESCAN: a server for the prediction and evaluation of "hot spots" of aggregation in polypeptides. BMC Bioinformatics 8, 65.
Cooper, E.A., Knutson, K., 1995. Fourier transform infrared spectroscopy investigations of protein structure. Pharm. Biotechnol. 7, 101–143.
de Vries, S.J., van Dijk, M., Bonvin, A.M., 2010. The HADDOCK web server for data-driven biomolecular docking. Nat. Protoc. 5, 883–897.
DePas, W.H., Chapman, M.R., 2012. Microbial manipulation of the amyloid fold. Res. Microbiol. 163, 592–606.
Divry, D., Florkin, M., 1927. Sur les proprietes optiques de l'amyloide. C.R. Soc. Biol. 97, 1808–1810.
Dobson, C.M., 1999. Protein misfolding, evolution and disease. Trends Biochem. Sci. 24, 329–332.
Donlan, R.M., 2002. Biofilms: microbial life on surfaces. Emerg. Infect. Dis. 8, 881–890.
Downing, D.T., Lazo, N.D., 1999. Molecular modelling indicates that the pathological conformations of prion proteins might be beta-helical. Biochem. J. 343 (Pt 2), 453–460.
Edwards, S.J., Kjellerup, B.V., 2013. Applications of biofilms in bioremediation and biotransformation of persistent organic pollutants, pharmaceuticals/personal care products, and heavy metals. Appl. Microbiol. Biotechnol. 97, 9909–9921.
Eswar, N., Webb, B., Marti-Renom, M.A., Madhusudhan, M.S., Eramian, D., Shen, M. Y., Pieper, U., Sali, A., 2006. Comparative protein structure modeling using Modeller. Curr. Protoc. Bioinformatics (Editoral board, Andreas D. Baxevanis et al., Chapter 5, Unit 5 6).
Evans, M.L., Chapman, M.R., 2013. Curli biogenesis: order out of disorder. Biochim. Biophys. Acta 1843, 1551–1558.
Fernandez-Escamilla, A.M., Rousseau, F., Schymkowitz, J., Serrano, L., 2004. Prediction of sequence-dependent and mutational effects on the aggregation of peptides and proteins. Nat. Biotechnol. 22, 1302–1306.
Fowler, D.M., Koulov, A.V., Alory-Jost, C., Marks, M.S., Balch, W.E., Kelly, J.W., 2006. Functional amyloid formation within mammalian tissue. PLoS Biol. 4, e6.
Galzitskaya, O.V., Garbuzynskiy, S.O., Lobanov, M.Y., 2006. Prediction of amyloidogenic and disordered regions in protein chains. PLoS Comput. Biol. 2, e177.
Geddes, A.J., Parker, K.D., Atkins, E.D., Beighton, E., 1968. "Cross-beta" conformation in proteins. J. Mol. Biol. 32, 343–358.
Hammar, M., Arnqvist, A., Bian, Z., Olsen, A., Normark, S., 1995. Expression of two csg operons is required for production of fibronectin- and congo red-binding curli polymers in *Escherichia coli* K-12. Mol. Microbiol. 18, 661–670.

Hammar, M., Bian, Z., Normark, S., 1996. Nucleator-dependent intercellular assembly of adhesive curli organelles in *Escherichia coli*. Proc. Natl. Acad. Sci. U.S.A. 93, 6562–6566.
Hammer, N.D., Schmidt, J.C., Chapman, M.R., 2007. The curli nucleator protein, CsgB, contains an amyloidogenic domain that directs CsgA polymerization. Proc. Natl. Acad. Sci. U.S.A. 104, 12494–12499.
Hammer, N.D., McGuffie, B.A., Zhou, Y., Badtke, M.P., Reinke, A.A., Brannstrom, K., Gestwicki, J.E., Olofsson, A., Almqvist, F., Chapman, M.R., 2012. The C-terminal repeating units of CsgB direct bacterial functional amyloid nucleation. J. Mol. Biol. 422, 376–389.
Hamodrakas, S.J., 1988. A protein secondary structure prediction scheme for the IBM PC and compatibles. Comput. Appl. Biosci. 4, 473–477.
Hinsen, K., 2000. The molecular modeling toolkit: a new approach to molecular simulations. J. Comput. Chem. 21, 79–85.
Howorka, S., 2011. Molecular assembly in natural and engineered systems. Preface. Prog. Mol. Biol. Transl. Sci. 103, xi–xii.
Iconomidou, V.A., Hamodrakas, S.J., 2008. Natural protective amyloids. Curr. Protein Pept. Sci. 9, 291–309.
Iconomidou, V.A., Vriend, G., Hamodrakas, S.J., 2000. Amyloids protect the silkmoth oocyte and embryo. FEBS Lett. 479, 141–145.
Iconomidou, V.A., Chryssikos, G.D., Gionis, V., Vriend, G., Hoenger, A., Hamodrakas, S.J., 2001. Amyloid-like fibrils from an 18-residue peptide analogue of a part of the central domain of the B-family of silkmoth chorion proteins. FEBS Lett. 499, 268–273.
Ivanova, M.I., Sievers, S.A., Sawaya, M.R., Wall, J.S., Eisenberg, D., 2009. Molecular basis for insulin fibril assembly. Proc. Natl. Acad. Sci. U.S.A. 106, 18990–18995.
Jorgensen, W.L., Tirado-Rives, J., 1988. The OPLS [optimized potentials for liquid simulations] potential functions for proteins, energy minimizations for crystals of cyclic peptides and crambin. J. Am. Chem. Soc. 110 (6), 1657–1666.
Kajava, A.V., Steven, A.C., 2006. Beta-rolls, beta-helices, and other beta-solenoid proteins. Adv. Protein Chem. 73, 55–96.
Kastritis, P.L., van Dijk, A.D., Bonvin, A.M., 2011. Explicit treatment of water molecules in data-driven protein-protein docking: the solvated HADDOCKing approach. Methods Mol. Biol. 819, 355–374.
Kim, C., Choi, J., Lee, S.J., Welsh, W.J., Yoon, S., 2009. NetCSSP: web application for predicting chameleon sequences and amyloid fibril formation. Nucleic Acids Res. 37, W469–W473.
Kitayama, H., Yoshimura, Y., So, M., Sakurai, K., Yagi, H., Goto, Y., 2013. A common mechanism underlying amyloid fibrillation and protein crystallization revealed by the effects of ultrasonication. Biochim. Biophys. Acta 1834, 2640–2646.
Kong, J., Yu, S., 2007. Fourier transform infrared spectroscopic analysis of protein secondary structures. Acta Biochim. Biophys. Sin. (Shanghai) 39, 549–559.
Krimm, S., Bandekar, J., 1986. Vibrational spectroscopy and conformation of peptides, polypeptides, and proteins. Adv. Protein Chem. 38, 181–364.
Larsen, P., Nielsen, J.L., Dueholm, M.S., Wetzel, R., Otzen, D., Nielsen, P.H., 2007. Amyloid adhesins are abundant in natural biofilms. Environ. Microbiol. 9, 3077–3090.
Lazo, N.D., Downing, D.T., 1998. Amyloid fibrils may be assembled from beta-helical protofibrils. Biochemistry 37, 1731–1735.
Lazo, N.D., Downing, D.T., 1999. Fibril formation by amyloid-beta proteins may involve beta-helical protofibrils. J. Pept. Res. 53, 633–640.
Leslie, A.G.W., Powell, H.R., 2007. Processing diffraction data with mosflm. In: Read, R., Sussman, J.L. (Eds.), Evolving Methods for Macromolecular Crystallography, vol. 245. Springer, Dordrecht, The Netherlands, pp. 41–51.
Loferer, H., Hammar, M., Normark, S., 1997. Availability of the fibre subunit CsgA and the nucleator protein CsgB during assembly of fibronectin-binding curli is limited by the intracellular concentration of the novel lipoprotein CsgG. Mol. Microbiol. 26, 11–23.
Lopez de la Paz, M., Serrano, L., 2004. Sequence determinants of amyloid fibril formation. Proc. Natl. Acad. Sci. U.S.A. 101, 87–92.
Louros, N.N., Iconomidou, V.A., 2015. Identification of an amyloid fibril forming segment of human Pmel17 repeat domain (RPT domain). Biopolymers 106, 133–139.
Louros, N.N., Iconomidou, V.A., Giannelou, P., Hamodrakas, S.J., 2013. Structural analysis of peptide-analogues of human Zona Pellucida ZP1 protein with amyloidogenic properties: insights into mammalian Zona Pellucida formation. PLoS One 8 e73258.
Louros, N.N., Petronikolou, N., Karamanos, T., Cordopatis, P., Iconomidou, V.A., Hamodrakas, S.J., 2014a. Structural studies of "aggregation-prone" peptide-analogues of teleostean egg chorion ZPB proteins. Biopolymers 102, 427–436.
Louros, N.N., Iconomidou, V.A., Tsiolaki, P.L., Chrysina, E.D., Baltatzis, G.E., Patsouris, E.S., Hamodrakas, S.J., 2014b. An N-terminal pro-atrial natriuretic peptide (NT-proANP) 'aggregation-prone' segment involved in isolated atrial amyloidosis. FEBS Lett. 588, 52–57.
Louros, N.N., Tsiolaki, P.L., Griffin, M.D., Howlett, G.J., Hamodrakas, S.J., Iconomidou, V. A., 2015a. Chameleon 'aggregation-prone' segments of apoA-I: a model of amyloid fibrils formed in apoA-I amyloidosis. Int. J. Biol. Macromol. 79, 711–718.
Louros, N.N., Tsiolaki, P.L., Zompra, A.A., Pappa, E.V., Magafa, V., Pairas, G., Cordopatis, P., Cheimonidou, C., Trougakos, I.P., Iconomidou, V.A., Hamodrakas, S.J., 2015b. Structural studies and cytotoxicity assays of "aggregation-prone" IAPP8-16 and its non-amyloidogenic variants suggest its important role in fibrillogenesis and cytotoxicity of human amylin. Biopolymers 104, 196–205.
Louros, N.N., Baltoumas, F.A., Hamodrakas, S.J., Iconomidou, V.A., 2016a. A beta-solenoid model of the Pmel17 repeat domain: insights to the formation of functional amyloid fibrils. J. Comput. Aided Mol. Des. 30, 153–164.
Louros, N.N., Chrysina, E.D., Baltatzis, G.E., Patsouris, E.S., Hamodrakas, S.J., Iconomidou, V.A., 2016b. A common 'aggregation-prone' interface possibly participates in the self-assembly of human zona pellucida proteins. FEBS Lett. 590, 619–630.
Maurer-Stroh, S., Debulpaep, M., Kuemmerer, N., Lopez de la Paz, M., Martins, I.C., Reumers, J., Morris, K.L., Copland, A., Serpell, L., Serrano, L., Schymkowitz, J.W., Rousseau, F., 2010. Exploring the sequence determinants of amyloid structure using position-specific scoring matrices. Nat. Methods 7, 237–242.
Missmahl, H.P., Hartwig, M., 1953. Polarisationsoptische Untersuchungen an der Amyloidsubstanz. Virchows Arch. 324, 489–508.
Nenninger, A.A., Robinson, L.S., Hultgren, S.J., 2009. Localized and efficient curli nucleation requires the chaperone-like amyloid assembly protein CsgF. Proc. Natl. Acad. Sci. U.S.A. 106, 900–905.
Oxford Diffraction, 2009. Chrysalis promotions. In: Diffraction (Ed.). Oxford Diffraction Ltd., Abingdon, Oxfordshire, England.
Pettersen, E.F., Goddard, T.D., Huang, C.C., Couch, G.S., Greenblatt, D.M., Meng, E.C., Ferrin, T.E., 2004. UCSF Chimera–a visualization system for exploratory research and analysis. J. Comput. Chem. 25, 1605–1612.
Richardson, J.S., Richardson, D.C., 2002. Natural beta-sheet proteins use negative design to avoid edge-to-edge aggregation. Proc. Natl. Acad. Sci. U.S.A. 99, 2754–2759.
Romhanyi, G., 1971. Selective differentiation between amyloid and connective tissue structures based on the collagen specific topo-optical staining reaction with Congo red. Virchows Arch. A Pathol. Pathol. Anat. 354, 209–222.
Savitsky, A., Golay, M.J.E., 1964. Smoothing and differentiation of data by simplified least-squares procedures. Anal. Chem. 36, 1627–1639.
Shewmaker, F., McGlinchey, R.P., Wickner, R.B., 2011. Structural insights into functional and pathological amyloid. J. Biol. Chem. 286, 16533–16540.
Shu, Q., Crick, S.L., Pinkner, J.S., Ford, B., Hultgren, S.J., Frieden, C., 2012. The *E. coli* CsgB nucleator of curli assembles to beta-sheet oligomers that alter the CsgA fibrillization mechanism. Proc. Natl. Acad. Sci. U.S.A. 109, 6502–6507.
Singh, R., Paul, D., Jain, R.K., 2006. Biofilms: implications in bioremediation. Trends Microbiol. 14, 389–397.
Sipe, J.D., Benson, M.D., Buxbaum, J.N., Ikeda, S., Merlini, G., Saraiva, M.J., Westermark, P., 2014. Nomenclature 2014: amyloid fibril proteins and clinical classification of the amyloidosis. Amyloid 21, 221–224.
Sunde, M., Serpell, L.C., Bartlam, M., Fraser, P.E., Pepys, M.B., Blake, C.C., 1997. Common core structure of amyloid fibrils by synchrotron X-ray diffraction. J. Mol. Biol. 273, 729–739.
Surewicz, W.K., Mantsch, H.H., Chapman, D., 1993. Determination of protein secondary structure by Fourier transform infrared spectroscopy: a critical assessment. Biochemistry 32, 389–394.
Teng, P.K., Anderson, N.J., Goldschmidt, L., Sawaya, M.R., Sambashivan, S., Eisenberg, D., 2012. Ribonuclease A suggests how proteins self-chaperone against amyloid fiber formation. Protein Sci. 21, 26–37.
Thompson, J.D., Higgins, D.G., Gibson, T.J., 1994. CLUSTAL W: improving the sensitivity of progressive multiple sequence alignment through sequence weighting, position-specific gap penalties and weight matrix choice. Nucleic Acids Res. 22, 4673–4680.
Tian, J., Wu, N., Guo, J., Fan, Y., 2009. Prediction of amyloid fibril-forming segments based on a support vector machine. BMC Bioinformatics 10 (Suppl. 1), S45.
Tian, P., Boomsma, W., Wang, Y., Otzen, D.E., Jensen, M.H., Lindorff-Larsen, K., 2015. Structure of a functional amyloid protein subunit computed using sequence variation. J. Am. Chem. Soc. 137, 22–25.
Tsolis, A.C., Papandreou, N.C., Iconomidou, V.A., Hamodrakas, S.J., 2013. A consensus method for the prediction of 'aggregation-prone' peptides in globular proteins. PLoS One 8 e54175.
Valery, C., Pandey, R., Gerrard, J.A., 2013. Protein beta-interfaces as a generic source of native peptide tectons. Chem. Commun. 49, 2825–2827.
Van Gerven, N., Klein, R.D., Hultgren, S.J., Remaut, H., 2015. Bacterial amyloid formation: structural insights into curli biogenesis. Trends Microbiol. 23, 693–706.
Vriend, G., 1990. WHAT IF: a molecular modeling and drug design program. J. Mol. Graph. Model. 8, 52–56, 29.
Wang, X., Chapman, M.R., 2008. Sequence determinants of bacterial amyloid formation. J. Mol. Biol. 380, 570–580.
Wang, X., Smith, D.R., Jones, J.W., Chapman, M.R., 2007. In vitro polymerization of a functional *Escherichia coli* amyloid protein. J. Biol. Chem. 282, 3713–3719.
Wang, X., Hammer, N.D., Chapman, M.R., 2008. The molecular basis of functional bacterial amyloid polymerization and nucleation. J. Biol. Chem. 283, 21530–21539.
Wang, X., Zhou, Y., Ren, J.J., Hammer, N.D., Chapman, M.R., 2010. Gatekeeper residues in the major curlin subunit modulate bacterial amyloid fiber biogenesis. Proc. Natl. Acad. Sci. U.S.A. 107, 163–168.
White, A.P., Collinson, S.K., Banser, P.A., Gibson, D.L., Paetzel, M., Strynadka, N.C., Kay, W.W., 2001. Structure and characterization of AgfB from *Salmonella enteritidis* thin aggregative fimbriae. J. Mol. Biol. 311, 735–749.
Wiltzius, J.J., Sievers, S.A., Sawaya, M.R., Cascio, D., Popov, D., Riekel, C., Eisenberg, D., 2008. Atomic structure of the cross-beta spine of islet amyloid polypeptide (amylin). Protein Sci. 17, 1467–1474.
Zhang, L., Zhu, X., Li, J., Liao, Q., Ye, D., 2011. Biofilm formation and electricity generation of a microbial fuel cell started up under different external resistances. J. Power Sources 196, 6029–6035.